

# Excited-State Photoelectron Spectroscopy of Excitons in Films of C<sub>60</sub> and Photopolymerized C<sub>60</sub>

J.P. Long, S.J. Chase, and M.N. Kabler

Naval Research Laboratory

Optoelectronic devices that employ organic semiconductors have recently appeared in commercial displays, and these devices also hold promise for use as lasers, inexpensive and mechanically flexible photovoltaics, and large-area photodetectors. When operating, these devices usually possess regions in which there occurs a complex mix of nonequilibrium states, including charge carriers (i.e., mobile electrons and holes) and neutral excitons. An exciton is an elementary excitation comprising an excited electron-hole pair bound together by mutual coulomb attraction. Unlike the delocalized and weakly bound excitons familiar in inorganic semiconductors, those in disordered organic materials tend to be confined to one or a few molecules and to be bound by several tenths of an electron volt. Molecular excitons are thus stable at room temperature until they spontaneously relax back to the ground state or are annihilated by collision interactions.

Low lying exciton states play important roles in molecular optoelectronic materials. Singlet excitons, in which the half-spins of the electron and hole combine for a total spin of zero, can couple to spin-zero photons. Hence, in general, it is the lowest lying of these singlet states, S<sub>1</sub>, that can emit light through radiative recombination. Singlet excitons are also generated with high efficiency by light absorption in photovoltaics and photodetectors, devices that must act to separate the electron-hole pair into charge carriers in order to drive external currents. In contrast to S<sub>1</sub> excitons, the lowest-lying spin-1 triplet excitons, T<sub>1</sub>, are largely dark. Lacking an efficient radiative recombination channel, triplets often have relatively long lifetimes. In addition, T<sub>1</sub> states, which lie lower in energy than S<sub>1</sub>, can form from S<sub>1</sub> through intersystem crossing. Their accumulation can decrease optical emission efficiency and can promote deleterious photochemical reactions.

Charge carriers and excitons can experience bimolecular collision interactions among themselves because, in general, they are mobile (although we find T<sub>1</sub> states to be relatively immobile in polymerized C<sub>60</sub>). Annihilation of one species often results from the collision, as represented by the well-documented interaction S<sub>1</sub>+S<sub>1</sub> → S<sub>1</sub> + S<sub>0</sub>, where S<sub>0</sub> represents the ground state [1]. Bimolecular interactions such as this become important at high concentrations and thus can limit the performance of devices such as lasers that operate at high excitation levels.

In spite of their importance, bimolecular interactions among multiple excited species are not understood in detail because it is experimentally difficult to detect simultaneously the various species with comparable sensitivity and time resolution. Thus even for a material as well studied as C<sub>60</sub>, questions remain concerning the nature of the photoexcited states and their dynamical interactions [2]. Excited-state photoelectron spectroscopy (ESPES) can offer advantages because it probes directly *all* nonequilibrium species containing an electron. In ESPES, a laser first excites a material and a subsequent photon probe photoemits electrons from the photoexcited populations into vacuum, where their relative kinetic energies are measured. Using both laser radiation (LR) and synchrotron radiation (SR) as time-resolved UV probes, we have applied ESPES to films of C<sub>60</sub> and photopolymerized C<sub>60</sub> (pp-C<sub>60</sub>), the latter more thoroughly because of larger signals [3, 4]. For the first time, S<sub>1</sub> and T<sub>1</sub> ESPES signals have been isolated and their dynamics followed in detail, with unexpected results.

Films of C<sub>60</sub>, 40-80 nm thick, were evaporated onto polished copper in UHV and studied *in situ* at beamline X24C at the NSLS. Pump-laser pulses from a copper-vapor laser (5-ns FWHM, 2.43-eV photon energy) at a 6-kHz rate were synchronized to the SR train *via* a trigger derived from a stripline signal [5]. SR was limited to energies below the cutoff of a LiF filter; without the filter, grating harmonics produced enough photoemission to obscure the weak ~1 Hz exciton signals. Metallic thin-film filters suitable for higher photon energies, even when used in conjunction with a critical-angle mirror [6], proved unable to attenuate higher orders enough while still providing usable signal levels.

Samples were photopolymerized with the same laser with samples held at room temperature; pristine films were studied at low temperature where the polymerization rate was negligible [7]. Photoelectron spectra were measured with a cylindrical mirror analyzer (CMA) at ~0.2 eV resolution. Signal counts from the CMA were time-resolved with a time-to-digital converter (TDC) and histogrammed within a time window referenced to the laser pulse. Single-bunch operations enhanced signal rates by reducing the duty-factor mismatch between laser and ring (1.76 MHz repetition rate in 1-bunch mode vs. 53 MHz in 25-bunch) and provided ~1-ns resolution through the usual pump-probe

method, wherein a controllable delay is introduced between laser pump and SR probe. In 25-bunch operations, the laser was desynchronized so that the ring served as a cw probe of exciton decays as recorded with the TDC. The 25-bunch operations allowed probing into the microsecond range, where long-lived  $T_1$  processes could be addressed.

SR data complemented in key ways the additional experiments conducted at NRL with laser radiation (LR). The LR setup employed harmonics of a Nd:YAG laser, the 2<sup>nd</sup> harmonic as pump (2.33 eV, 75 ps) and the 5<sup>th</sup> as probe (5.84 eV, ~50 ps) [4]. Figure 1 summarizes the spectroscopy of excitons in  $C_{60}$  and pp- $C_{60}$  recorded with both setups. Blue shading distinguishes SR data

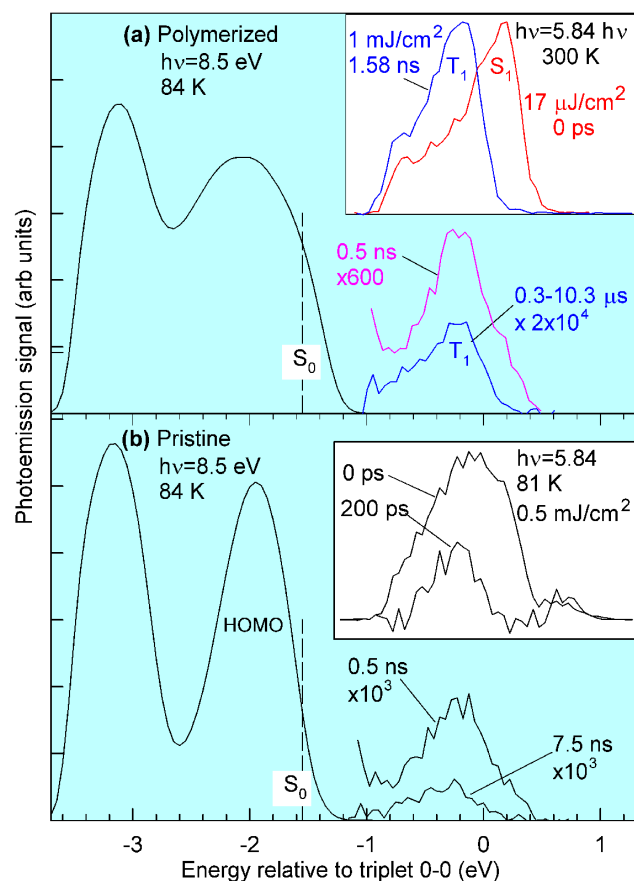


**Figure 1.** Photoelectron spectra of valence and background-subtracted excited states, probed with two sources: nanosecond synchrotron (blue shaded,  $2.8 \text{ mJ/cm}^2$ ) and picosecond laser (insets). Zero energy is the estimated 0-0 line of triplet exciton  $T_1$ . (a) pp- $C_{60}$ . Note pure  $T_1$  spectrum accumulated from 0.3 to 10.3  $\mu\text{s}$  after 5-ns pump pulse. The 0.5-ns spectrum comprises both  $S_1$  and  $T_1$ . Inset: pp- $C_{60}$  comparing normalized  $S_1$  at low fluence to nearly pure  $T_1$  after high-fluence dynamic interactions. (b) Pristine  $C_{60}$ .

in all figures. Excited-state emission appears at energies above  $-1 \text{ eV}$ . This emission falls mostly below the Fermi level  $E_F$  and hence is from electrons that had been bound in excitons ( $E_F$  fell between 0.3 and 0.4 eV for all data). We were able to assign  $T_1$  unambiguously, and correct an earlier ESPES assignment [8], by employing SR in 25-bunch mode to probe at such long times that only  $T_1$  states remained. The blue spectrum in Figure 1a shows pure  $T_1$  emission from pp- $C_{60}$  recorded between 0.3 and 10.3  $\mu\text{s}$  after the pump-laser pulse, times much longer than the  $S_1$  unimolecular lifetime of only 1.3 ns. The purple spectrum was recorded in 1-bunch operations with laser and synchrotron pulses *coincident* in time. The excess emission appearing on the high-energy side was revealed to be  $S_1$  by probing with picosecond LR at a time much less than the intersystem crossing time of  $\sim 2.5 \text{ ns}$  and, at the same time, using low pump fluence (red spectrum in the inset to Figure 1a). Surprisingly, at larger fluences the  $T_1$  population was favored over  $S_1$ , even at times much less than the intersystem crossing time, because of collision interactions discussed below. Under these conditions, bimolecular interactions rapidly annihilated  $S_1$  so that a  $T_1$  spectrum could be isolated after only  $\sim 1.6 \text{ ns}$ , as shown by the blue curve in the inset to Figure 1a.

Use of SR at 8.5 eV permitted recording a spectrum comprising *both* ground-state valence band and excitons from the same film. This led to a significant insight regarding the location of the origin of transitions within the highest occupied molecular orbital (HOMO). The energy of a photoemission 0-0 transition (i.e., with no vibrations involved) can be estimated if the emission displays a characteristic vibronic lineshape [9]. The HOMO photoemission from  $C_{60}$  films does not. However, in Figure 1a, the Poisson-shaped  $T_1$  spectrum isolated at late time with SR does indeed exhibit a vibrationally broadened lineshape, as do the identically shaped  $S_1$  and  $T_1$  spectra in the inset. Locating the 0-0 transition within the upper limb of these lineshapes [9] is the basis for the energy zero of Figure 1. Using reported 0-0 creation energies for  $T_1$  ( $\sim 1.54 \text{ eV}$ ) or  $S_1$  ( $\sim 1.87 \text{ eV}$ ) in  $C_{60}$ , and noting the identical exciton energetics between  $C_{60}$  and pp- $C_{60}$ , we can then locate the origin of transitions, labeled  $S_0$  in Figure 1 [3, 4]. It is important to note that  $S_0$  is not centered on the HOMO photoemission band, but occurs near its upper edge. This result determines in a new way the alignment between  $S_0$  and the Fermi level at  $\sim 0.35 \text{ eV}$  and emphasizes the care needed when interpreting photoemission spectra, e.g. to estimate injection barriers between metallic contacts and molecular levels.

The prominent  $T_1$  contribution to the purple curve of Figure 1, recorded with SR about 2 ns into the pump-laser pulse when  $S_1$  would also be expected to be strong, is due in part to an effective conversion of  $S_1$  to

$T_1$  states. This conversion occurs at high excitation due to collision interactions, as noted above [3, 4]. The conversion was suggested by SR measurements of the fluence-dependent emission recorded at different kinetic energies within the exciton spectrum as given in Figure 2. Relative to the slope of the pure  $S_1$  emission (red) measured at higher kinetic energy, the stronger slope of the purple data, measured at the peak of the spectrum (see inset), where both  $S_1$  and  $T_1$  contribute, is caused by a  $T_1$  contribution that increases disproportionately with fluence. Solid lines give results of a rate-equation model incorporating bimolecular collisions [3]. The enhanced  $T_1$  production at high concentration becomes convincing with use of LR, as shown in Figure 3, where the fluence dependences of the  $S_1$  and  $T_1$  contributions to the full exciton spectrum are displayed. Figure 3 also displays emission  $\sim 0.5$  eV above  $S_1$ , which we attribute to mobile or trapped unbound electrons, although charge-transfer excitons cannot be ruled out. This higher lying emission was too weak to observe with SR or to study in detail with the LR setup.

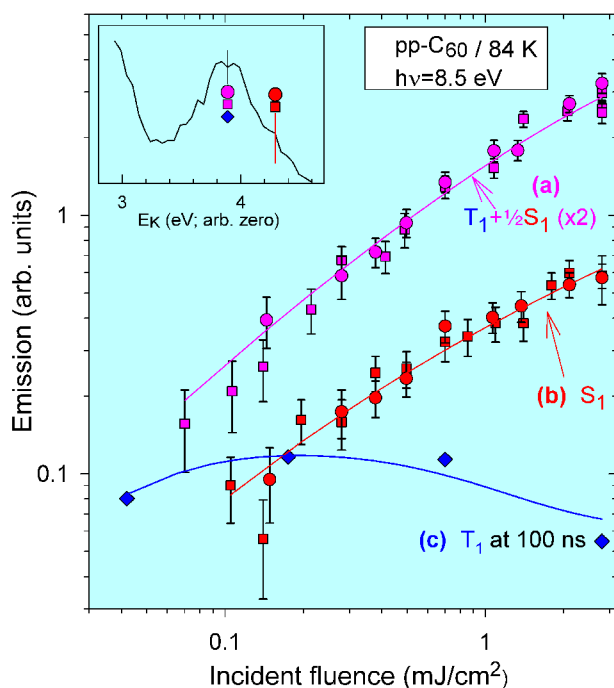


**Figure 2.** Pump-laser fluence dependence of exciton emission at the two kinetic energies denoted in the inset as measured with synchrotron radiation. Red symbols: kinetic energy selected for essentially pure  $S_1$  (single bunch operations). Purple symbols: peak of spectrum, where both  $T_1$  and  $S_1$  contribute (single bunch). Blue symbols: peak of spectrum, but measured at a 100-ns delay when only  $T_1$  excitons contribute (25-bunch operations). Solid lines give results of a rate equation model discussed in text.

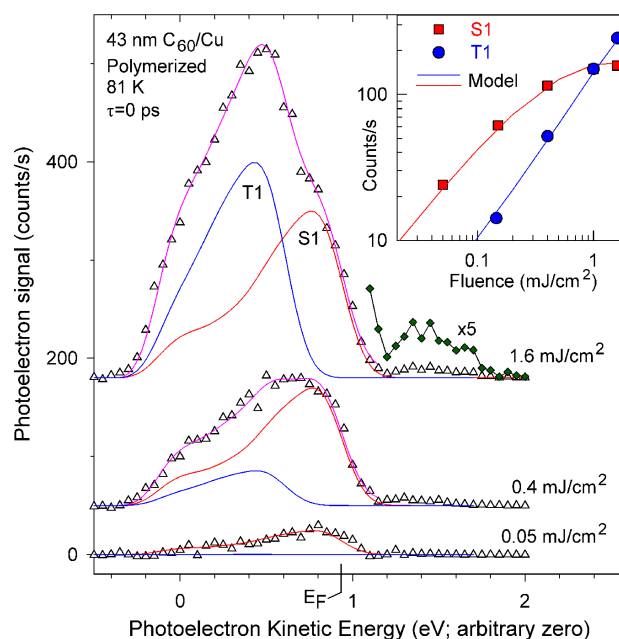


**Figure 3.** Pump-laser fluence dependence of the exciton spectrum as measured with Nd:YAG laser radiation. Symbols: background-subtracted spectra for various incident fluences of the 75-ps pump laser when coincident with the probe pulse ( $\tau=0$ ). Spectra are offset vertically for clarity.  $T_1$  predominance at high fluence is evident as the increasing peak at 0.5 eV. The emission band (green) above the measured Fermi level  $E_F$  is located approximately at the lowest unoccupied molecular orbital. Curves: fits of  $S_1$  and  $T_1$  contributions using an identical model-lineshape for both excitons. Inset: Symbols give fluence dependence of  $S_1$  and  $T_1$  from the fitted components; curves give results of a rate-equation model [3].

In Figure 2, blue diamonds show that as pump fluence increases, an intriguing decrease occurs in the late-time  $T_1$  population. The solid blue line gives results of the rate equation model, which indicates that this surprising behavior is the result of  $T_1$  annihilation by mobile charge carriers. These late-time data were obtained from decay curves measured in 25-bunch mode; examples are given in Figure 4. Two factors, our limited time resolution in 25-bunch mode [5] and data smoothing, distort the rapidly varying behavior near the pump pulse at 0 ns. Nonetheless, the crossing of the upper two traces in Figure 4 demonstrates marked “non-Markovian” behavior in the sense that the decay rate is not strictly a function of exciton density (which is approximately equal for the two decays at the crossing point), but depends on history [2, 10].

To fit a wide range of fluence- and time-dependent data from pp- $C_{60}$  with the rate equation model mentioned above, we found it necessary to include bimo-

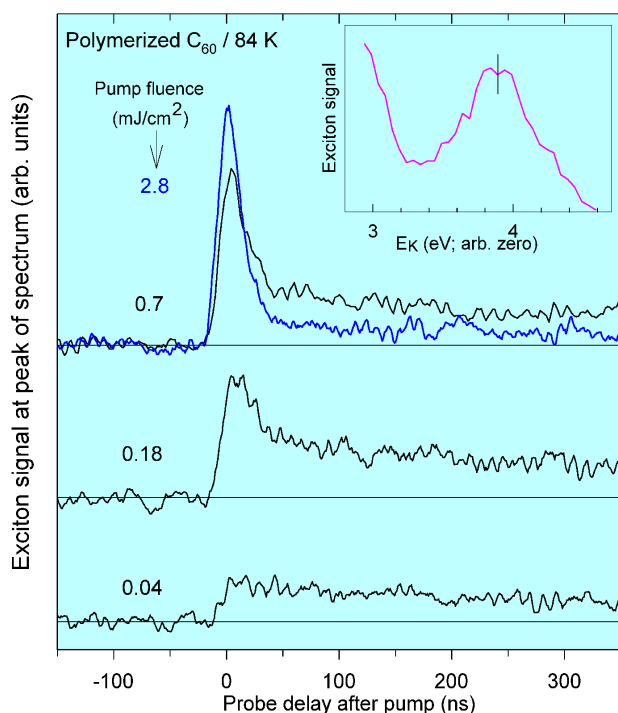


**Figure 4.** Dependence of long-term exciton decay on pump-laser fluence, as measured with synchrotron radiation in 25-bunch operations. Inset shows the kinetic energy within the exciton spectrum at which decays were recorded. With a maximum lifetime of 1.3 ns, singlet  $S_1$  excitons contribute only at the shortest times near the laser pulse at 0 delay. Note that the 2.8 mJ/cm<sup>2</sup> decay curve (blue) crosses beneath the lower fluence, 0.7 mJ/cm<sup>2</sup> decay.

molecular interactions among all three of the lowest lying nonequilibrium species, i.e., charge carriers, and  $S_1$  and  $T_1$  excitons [3]. As noted above, annihilation of  $T_1$  by collisions with charge carriers proved necessary to reproduce the crossing decays of Figure 4. The enhanced production of  $T_1$  observed at elevated excited-state concentrations ( $>3 \times 10^{19} \text{ cm}^{-3}$ ), another significant finding, could be reproduced by invoking the interaction  $S_1 + S_1 \rightarrow T_1 + T_1$  or, with greater accuracy, by a novel intersystem crossing catalyzed by charge-carrier collisions:  $C + S_1 \rightarrow C + T_1$ . For the case of pristine  $C_{60}$ , weaker signals due to more rapid decays, and sample-to-sample variability, precluded a similarly detailed analy-

sis. However, the more rapid  $C_{60}$  dynamics, which are probably a consequence of larger excited-state mobilities, were qualitatively similar to pp- $C_{60}$ . In addition, almost identical energetics are apparent for the two phases (Figure 1). Further discussion of the rate equation model is beyond the scope of this highlight article.

The present work demonstrates that ESPES, by directly measuring multiple excited species in molecular films, can disclose complex excited-state behavior that is likely to complicate device performance at high concentrations. To summarize, the more notable results are [3, 4]: (i) the first isolation and correct assignments of  $S_1$ - and  $T_1$ -exciton photoemission spectra in any material; (ii) the unusual observation of vibrationally broadened photoemission from the solid state, in this case from  $T_1$  and  $S_1$  excitons; (iii) location of the origin of transitions at the top of the HOMO; (iv) the interesting discovery that production of  $T_1$  excitons is enhanced for large excited-state concentrations, with potential implications for optoelectronic devices; (v) marked non-Markovian  $T_1$  decays; and (vi) evidence for charge-carrier annihilation of excitons.

## References

- [1] M. Pope and C.E. Swenberg, *Electronic Processes in Organic Crystals and Polymers* (Oxford University Press, New York, 1999).
- [2] S.L. Dexheimer, in *Optical and Electronic Properties of Fullerenes and Fullerene-Based Materials*, edited by J. Shinar, Z. V. Vardeny and Z. H. Kafafi (Marcel Dekker, Inc., New York, 2000), p. 21.
- [3] J.P. Long, S.J. Chase, and M.N. Kabler, *Chem. Phys. Lett.* **347**, 29 (2001).
- [4] J.P. Long, S.J. Chase, and M.N. Kabler, *Phys. Rev. B* **64**, 205415 1 (2001).
- [5] J.P. Long, *Nucl. Instrum. Methods Phys. Res.* **A266**, 673 (1988).
- [6] W. R. Hunter and J.P. Long, *Appl. Optics* **33**, 1264 (1994).
- [7] B.S. Itchkawitz, J.P. Long, T. Schedel-Niedrig, M.N. Kabler, A.M. Bradshaw, R. Schloegl, and W.R. Hunter, *Chem. Phys. Lett.* **243**, 211 (1995).
- [8] R. Jacquemin, S. Kraus, and W. Eberhardt, *Solid State Commun.* **105**, 449 (1998).
- [9] P.A. Brühwiler, A.J. Maxwell, P. Baltzer, S. Andersson, D. Arvanitis, L. Karlsson, and N. Mårtensson, *Chem. Phys. Lett.* **279**, 85 (1997).
- [10] S.L. Dexheimer, W. A. Vareka, D. Mittleman, A. Zettl, and C.V. Shank, *Chem Phys Lett* **235**, 552 (1995).